

Article

# Ru/Pd Complex and Its Monometallic Fragments as Catalysts for Norbornene Polymerization via ROMP and Addition

Thaís R. Cruz <sup>1</sup>, Gustavo H. C. Masson <sup>1</sup>, Kelly A. E. Amorim <sup>2</sup>, Antonio E. H. Machado <sup>3,4</sup> , Beatriz E. Goi <sup>1</sup> and Valdemiro P. Carvalho-Jr. <sup>1,\*</sup>

<sup>1</sup> Faculdade de Ciências e Tecnologia, UNESP—Univ. Estadual Paulista, Presidente Prudente 19060-900, SP, Brazil

<sup>2</sup> Instituto de Química de São Carlos, Universidade de São Paulo, São Carlos 13560-970, SP, Brazil

<sup>3</sup> Instituto de Química, Universidade Federal de Uberlândia, Uberlândia 38400-089, MG, Brazil

<sup>4</sup> Instituto de Física, Programa de Pós-Graduação em Ciências Exatas e Tecnológicas, Universidade Federal de Catalão, Catalão 75704-020, GO, Brazil

\* Correspondence: valdemiro.carvalho@unesp.br

**Abstract:** The [Ru(PPh<sub>3</sub>)<sub>2</sub>Cl-piperidine(4-aminomethyl)] complex (mono-Ru) was synthesized from [Ru(PPh<sub>3</sub>)<sub>3</sub>Cl<sub>2</sub>] and 4-(aminomethyl)piperidine, whereas the [(PPh<sub>3</sub>)PdCl(Schiff-pip)] complex (mono-Pd) was obtained by reacting [Pd(PPh<sub>3</sub>)<sub>2</sub>Cl<sub>2</sub>] with its respective Schiff base ligand, both at a 1:1 molar ratio. The heterobimetallic [RuCl<sub>2</sub>(PPh<sub>3</sub>)<sub>2</sub>](μ-Schiff)Pd(PPh<sub>3</sub>)Cl complex (Ru/Pd) was synthesized via a one-pot, three-component reaction of mono-Ru, [(Pd(PPh<sub>3</sub>)<sub>2</sub>Cl<sub>2</sub>] and salicylaldehyde. All complexes were fully characterized by FTIR, UV-Vis, and NMR spectroscopy, as well as elemental analysis, MALDI-TOF mass spectrometry, cyclic voltammetry, and computational studies. Ru/Pd was able to polymerize norbornene (NBE) by two different mechanisms: ROMP and vinyl polymerization. The Ru fragment was active for ROMP of NBE, reaching yields of 68 and 31% for mono-Ru and Ru/Pd, respectively, when the [NBE]/[Ru] = 3000 molar ratio and 5 μL EDA addition were employed at 50 °C. The poly(norbornene) (polyNBE) obtained presented an order of magnitude of 10<sup>4</sup> g mol<sup>-1</sup> and Đ values between 1.48 and 1.79. For the vinyl polymerization of NBE, the Pd fragment was active using MAO as a cocatalyst, reaching a yield of 47.0% for Ru/Pd and quantitative yields for mono-Pd when [Al]/[Pd] = 2500 and [NBE]/[Pd] = 20,000 molar ratios were employed, both at 60 °C.

**Keywords:** heterobimetallic complexes; metathesis; bifunctional catalysts; ruthenium; palladium



**Citation:** Cruz, T.R.; Masson, G.H.C.; Amorim, K.A.E.; Machado, A.E.H.; Goi, B.E.; Carvalho-Jr., V.P. Ru/Pd Complex and Its Monometallic Fragments as Catalysts for Norbornene Polymerization via ROMP and Addition. *Catalysts* **2022**, *12*, 1111. <https://doi.org/10.3390/catal12101111>

Academic Editor: Francisco J. Fernández-Alvarez

Received: 1 July 2022

Accepted: 13 September 2022

Published: 26 September 2022

**Publisher's Note:** MDPI stays neutral with regard to jurisdictional claims in published maps and institutional affiliations.



**Copyright:** © 2022 by the authors. Licensee MDPI, Basel, Switzerland. This article is an open access article distributed under the terms and conditions of the Creative Commons Attribution (CC BY) license (<https://creativecommons.org/licenses/by/4.0/>).

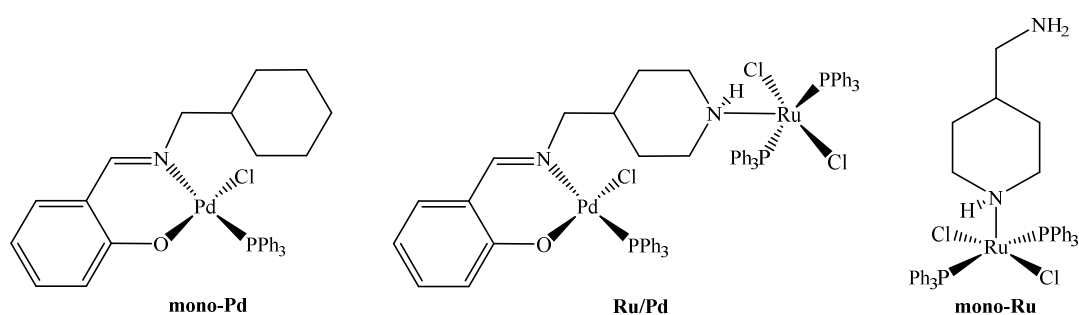
## 1. Introduction

Complexes based on late-transition metals have been widely used as catalysts in a large number of catalytic reactions, such as the reactions of olefins and acetylenes with hydrogen, carbon monoxide, water, or other nucleophiles, as well as the isomerization, oligomerization, and polymerization of olefins [1,2]. Especially, ruthenium (Ru) and palladium (Pd) metallic centers have emerged as multifunctional catalysts [3–11]. These transition-metals have demonstrated high catalytic activity in polymerization reactions [11]. Based on the functionality of these metals, and aiming to increase the range of catalytic reactions, a large number of studies using heterobimetallic complexes composed of Ru(II) and Pd(II) fragments have been conducted [11–13]. Furthermore, the use of bimetallic complexes as homogeneous catalysts can increase reactivity via synergistic cooperation [14,15].

A well-defined macromolecular structure is certainly a goal in synthetic polymer chemistry. Ring-opening metathesis polymerization (ROMP) is a good alternative process that can produce high molecular weight and unsaturated polymers from a cyclic olefin, while vinyl polymerization can produce long saturated polymers [16–18]. Ruthenium-catalyzed ROMP of norbornene is particularly interesting to obtain unsaturated poly(norbornene) (polyNBE), since it presents high selectivity for olefins and has an electron-rich metallic center [19]. The principal application of these polymers is in the Norsorex<sup>®</sup> process [20].

PolyNBE can also be obtained by vinyl polymerization using Pd complexes as catalysts. Through this method, it is possible to obtain linear polymers with high molecular weight and saturated chains without the opening ring process [21,22]. Thus, the properties of this polymer are different from those obtained by ROMP, with emphasis on its high heat resistivity and mechanical resistance [20].

In studies conducted by our research group, ROMP has been initiated using non-carbene amine-based Ru complexes, where the active species is obtained in situ through reaction between the Ru complex and ethyl diazoacetate (EDA) [11,23–27]. Recently, heterobimetallic systems for multifunctional catalysts, mainly in the polymerization mechanism, have been addressed [11,28]. This study reports on the synthesis and characterization of a new heterobimetallic complex based on Ru(II) and Pd(II) for ROMP and vinyl polymerization of norbornene. This catalyst was designed to contain a phosphine-Ru(II) fragment to initiate the ROMP reactions and phosphine-Pd(II)-(N,O-Schiff) fragment to initiate the vinyl polymerization reactions (Scheme 1). In addition, the Ru(II) and Pd(II) monometallic fragments were synthesized to relate the catalytic activity to each metallic center and their contributions to the reactions.

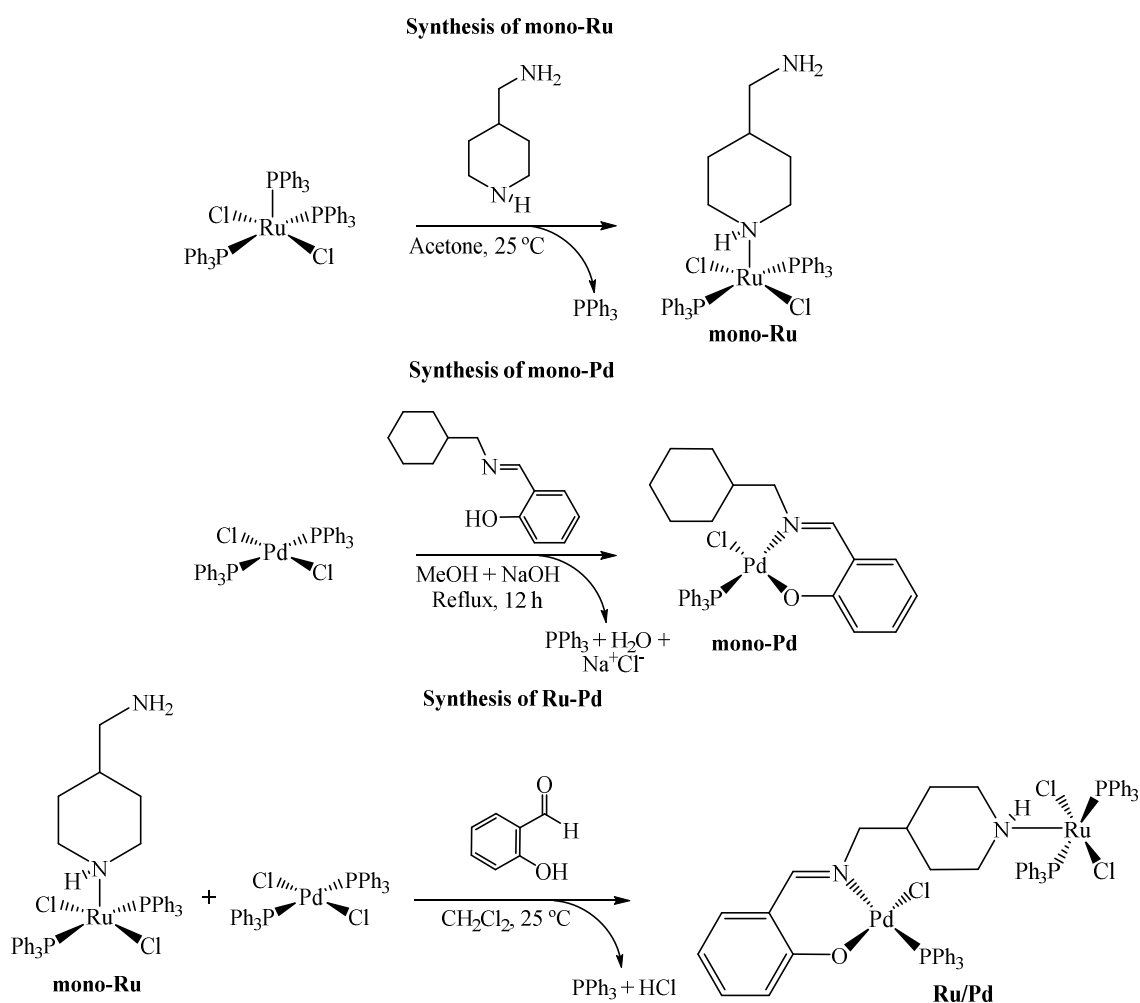


**Scheme 1.** The Ru/Pd heterobimetallic complex and its monometallic fragments: mono-Pd and mono-Ru.

## 2. Results and Discussion

### 2.1. Synthesis and Characterization

Mono-Pd was prepared from the reaction of  $[\text{Pd}(\text{PPh}_3)_2\text{Cl}_2]$  with 1 equiv. of Schiff base in methanol under reflux for 12 h to obtain a dark yellow solid (Scheme 2). Prior to the complexation step, the Schiff base ligand was suspended in MeOH and deprotonated with sodium hydroxide at room temperature. Mono-Ru was prepared from the rapid reaction of the  $[\text{Ru}(\text{PPh}_3)_3\text{Cl}_2]$  precursor complex with 1 equiv. of 4-(aminomethyl)piperidine in acetone to generate the light pink solid (Scheme 2). The heterobimetallic  $[\text{RuCl}_2(\text{PPh}_3)_2](\text{-Schiff})\text{Pd}(\text{PPh}_3)\text{Cl}]$  complex (Ru/Pd) was obtained from the reaction between mono-Ru,  $[\text{Pd}(\text{PPh}_3)_2\text{Cl}_2]$  and salicylaldehyde (1:1:1 equiv.) to obtain a Schiff base (N,N,O) via one-pot three-component synthesis, which linked the monometallic fragments (Scheme 2). Mono-Ru, mono-Pd, and Ru/Pd were characterized by elemental analysis, spectroscopic techniques, cyclic voltammetry, and density functional theory (DFT) calculations. All attempts to obtain crystals for X-ray diffraction (XRD) studies have not been successful so far.



**Scheme 2.** Overview of reactions to obtain mono-Ru, mono-Pd, and Ru/Pd.

The elemental analyses of mono-Ru, mono-Pd, and Ru/Pd agreed well with the molecular formula predicted for these compounds. The FTIR spectrum of mono-Ru revealed two large bands around  $3255\text{ cm}^{-1}$  from asymmetric  $\nu(\text{N-H})$  stretching, indicating that 4-(aminomethyl)piperidine was coordinated to  $[\text{Ru}(\text{PPh}_3)_3\text{Cl}_2]$  (Figure S1). The spectra of both mono-Pd and Ru/Pd showed characteristic absorption bands at  $1620$  and  $1622\text{ cm}^{-1}$ , respectively, from  $\nu(\text{C=N})$  stretching. These values are different from that of the free Schiff base, which appeared at  $1619\text{ cm}^{-1}$ , indicating that the ligand is coordinated by iminic nitrogen in mono-Pd and Ru/Pd. The  $\nu(\text{Pd-Cl})$  and  $\nu(\text{Ru-Cl})$  stretches in Ru/Pd at  $340$  and  $298\text{ cm}^{-1}$ , respectively, and suggesting the presence of two different metal centers in this heterobimetallic compound (Figure S1).

The  $^1\text{H}$  NMR spectra of mono-Ru and Ru/Pd exhibit peaks in the  $0.48$ – $3.51$  ppm range as multiplets assigned to the  $\text{CH}_2$  hydrogen groups from the amine ring in the Ru center (Figures S2 and S4). Additionally, mono-Ru shows a triplet around  $3.75$  ppm, assigned to the  $\text{NH}_2$  protons from the primary amine. In Ru/Pd, the disappearance of the signal of the  $\text{NH}_2$  protons, followed by the appearance of a multiplet around  $6.78$  ppm for the  $\text{H-C=N}$  group proton, suggests the formation of azomethine nitrogen in Ru-Pd. As for mono-Pd and Ru/Pd (Figure S4), the signal of the azomethine nitrogen merges with the phosphine protons (Figures S3 and S4). The multiplet around  $3.48$  ppm is assigned to the  $\text{NH}$  group from the secondary amine for both mono-Ru and Ru/Pd. The  $^1\text{H}$  NMR spectrum of mono-Pd shows multiplets in the  $0.89$ – $2.00$  ppm range for the amine ring protons. Mono-Pd, Ru/Pd, and mono-Ru show multiplets between  $2.00$ – $0.80$  ppm, which are assigned to the  $\text{CH}_2$  from the primary amine. The peaks in the  $6.55$ – $7.30$  ppm range

for mono-Ru and Ru/Pd are assigned to the phenyl segment from the Schiff base ligand. The  $^1\text{H}$  NMR spectra of mono-Ru, mono-Pd, and Ru/Pd exhibit signals for the phosphine protons as multiplets in the 5.50–7.80 ppm range.

The  $^{31}\text{P}\{^1\text{H}\}$  NMR spectra show a singlet at 23.22 ppm for mono-Pd and two singlets at 62.19 and 44.38 ppm for mono-Ru assigned to the square-based pyramid and trigonal bipyramidal structures, as previously reported (Figures S5 and S6) [29]. The  $^{31}\text{P}\{^1\text{H}\}$  NMR spectrum for Ru/Pd exhibits a peak at 23.12 ppm, consistent with the presence of the Pd fragment in the new species formed (Figure S7). This spectrum also shows a number of signals that can be associated with the presence of different Ru species in the solution. The two peaks at 66.23 and 44.18 ppm in the spectrum confirm the presence of the two structural isomers for the Ru fragment in Ru/Pd, as observed for mono-Ru. The singlet at  $-4.90$  ppm is typical of free  $\text{PPh}_3$ . This is a clear indication of the release of  $\text{PPh}_3$  from Ru/Pd, suggesting the formation of a dimeric species with one singlet at 40.0 ppm. The free  $\text{PPh}_3$  and Ru center can undergo a reaction with residual  $\text{O}_2$  to produce  $\text{OPPh}_3$  and other Ru species, with sharp peaks at 29.10 and 34.00 ppm, respectively (Figure S7).

The MALDI-TOF mass spectrometry analyses of mono-Ru and Ru/Pd were recorded in  $\text{CH}_2\text{Cl}_2$ . The mass spectrum of mono-Ru exhibited a peak corresponding to the  $[\text{mono-Ru}] + \text{H}^+$ , confirming the formation of the expected mononuclear Ru complex (Figure S8). Ru/Pd exhibited a signal at 13,170,373  $m/z$  consistent with  $[\text{Ru/Pd}] + \text{H}^+$ , thus providing strong evidence for the formulation proposed for this heterobimetallic complex (Figure S9).

Computational studies were carried out on the monometallic and heterobimetallic complexes. Theoretical details, involving the selected bond distances and bond angles, are shown in Table 1, and the optimized structures proposed for mono-Pd, mono-Ru, and Ru/Pd are shown in Figure 1. The geometrical parameters of mono-Ru revealed a distorted square-based pyramid similar to those previously reported [30]. Analysis of the P–Ru–P angle shows a value of  $163^\circ$ , indicating *trans*-positioned phosphines in a distorted geometry. Mono-Pd showed a typical distorted square planar molecular geometry, where the N–Pd–O bond angle and Pd–P bond distance have values close to those predicted for similar complexes [11,19,31,32]. The bond angle and distance values of the monometallic complexes and their fragments in the heterobimetallic species were very similar. This similarity shows that the geometry of the Ru and Pd fragments is conserved in the formation of Ru/Pd.

**Table 1.** Theoretical bond distances (Å) and bond angles ( $^\circ$ ) for mono-Ru, mono-Pd, and Ru/Pd.

Geometric Parameters	mono-Ru	Ru/Pd	mono-Pd
Ru(1)–Cl(1)	2.4492	2.4528	-
Ru(1)–Cl(2)	2.4510	2.4623	-
Ru(1)–P(1)	2.4497	2.4539	-
Ru(1)–P(2)	2.4583	2.4308	-
Ru(1)–N(1)	2.1425	2.1361	-
Cl(1)–Ru(1)–Cl(2)	168.420	170.521	-
Cl(1)–Ru(1)–N(1)	85.655	85.857	-
Cl(2)–Ru(1)–N(1)	98.720	103.557	-
P(1)–Ru(1)–P(2)	163.994	162.371	-
Pd(1)–Cl(3)	-	2.3583	2.3580
Pd(1)–N(2)	-	2.0755	2.0773
Pd(1)–O(1)	-	2.0224	2.0172
Pd(1)–P(3)	-	2.2953	2.2971
N(2)–Pd(1)–O(1)	-	89.251	89.664
P(3)–Pd(1)–Cl(3)	-	86.590	86.369

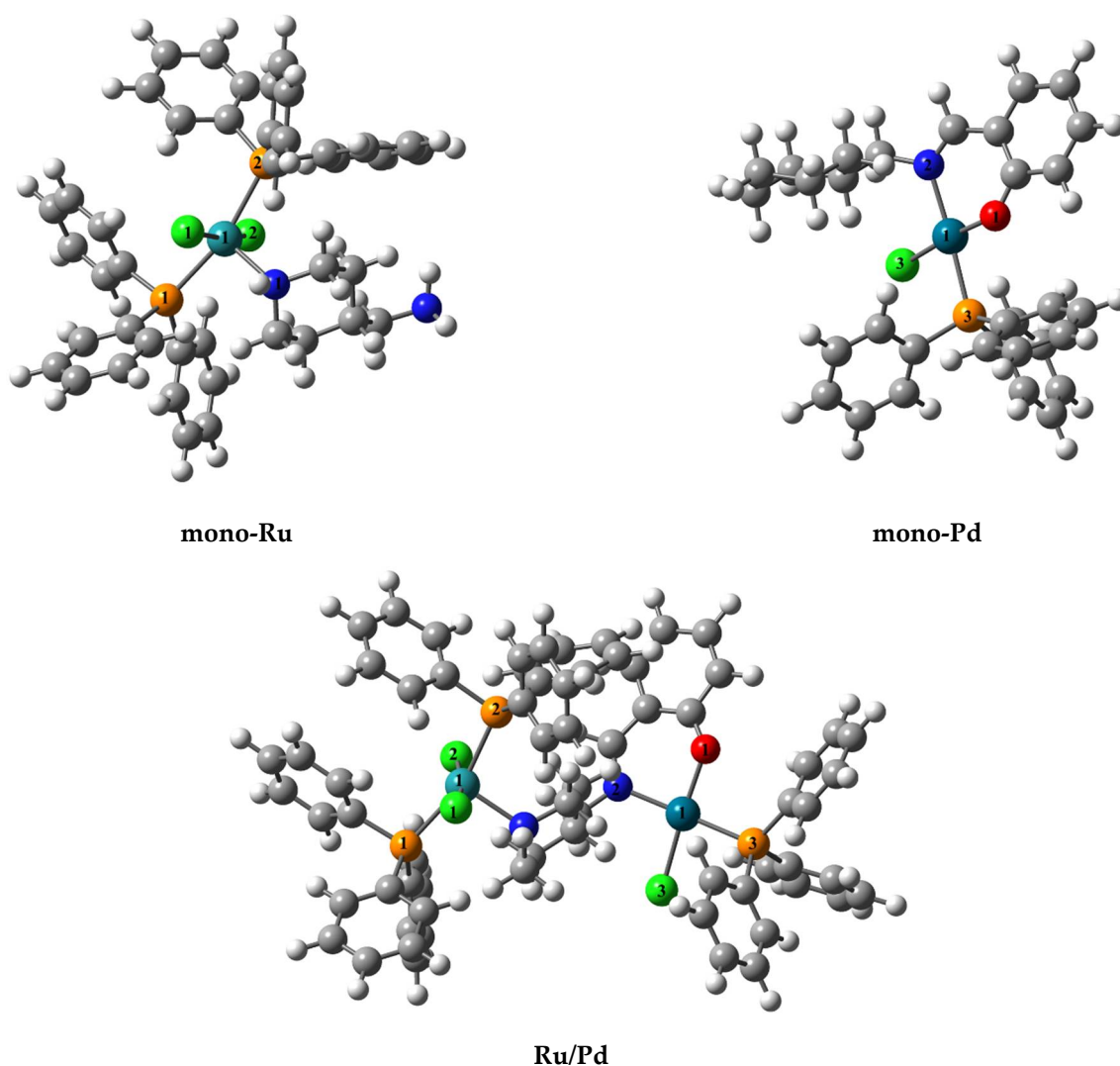


**Figure 1.** Views of the optimized structures of mono-Pd, mono-Ru, and Ru/Pd.

The UV-vis absorption spectra of mono-Ru, mono-Pd, and Ru/Pd showed two intense absorption bands in the 200–300 nm range related to the intraligand (IL) transfer. MLCT bands can be observed for mono-Ru ( $\lambda_{\max}$  at 346 nm) and mono-Pd ( $\lambda_{\max}$  at 343 and 394 nm), and they are assigned to  $d \rightarrow \pi^*$  charge transfer transitions. Both monometallic complexes showed bands related to the metallic center or the  $d-d$  charge transfer with  $\lambda_{\max}$  at 640 and 636 nm for mono-Ru and mono-Pd, respectively. All bands observed in the monometallic species were also observed in Ru/Pd, with a bathochromic shift (red shift). The  $\lambda_{\max}$  shift on the absorption spectrum of Ru/Pd confirms that the reaction between mono-Ru,  $[\text{Pd}(\text{PPh}_3)_2\text{Cl}_2]$ , and salicylaldehyde resulted in a new species containing fragments of both monometallic species. The theoretical absorption spectrum for Ru/Pd was obtained from DFT calculations with dichloromethane as a solvent (Figure 2). The theoretical and experimental absorption spectra of the heterobimetallic species shown in Figure 2 are in excellent agreement. The comparative similarity between the theoretical and experimentally calculated oscillator strengths for Ru/Pd provides reliability to the analysis of the theoretically predicted structure.

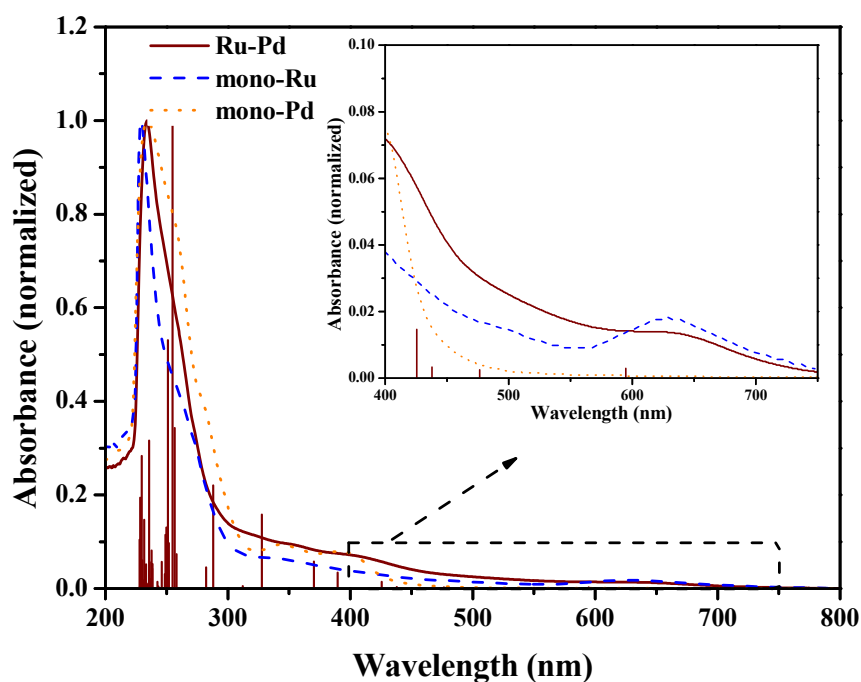


**Figure 2.** Electronic absorption spectra of mono-Ru (blue dashed line), mono-Pd (orange dotted line), and Ru-Pd (marron solid line) and experimentally calculated oscillator strength ( $f$ ) (dark red vertical lines) for Ru-Pd. Conditions:  $[Ru/Pd] = [mono-Ru] = [mono-Pd] = 1.0 \times 10^{-4} \text{ mol L}^{-1}$ ;  $\text{CH}_2\text{Cl}_2$  as solvent, at  $25^\circ\text{C}$ .

Formal oxidation and reduction potentials of mono-Ru, mono-Pd, and Ru/Pd vs. Ag/AgCl were obtained from cyclic voltammograms recorded on a platinum electrode in  $\text{CH}_2\text{Cl}_2$  containing  $0.1 \text{ mol L}^{-1}$  tetrabutylammonium hexafluorophosphate ( $n\text{-Bu}_4\text{NPF}_6$ ) as a supporting electrolyte. Mono-Ru showed an irreversible oxidation peak at  $0.63 \text{ V}$  attributed to the metal-centered oxidation of  $\text{Ru}^{\text{II/III}}$ , while mono-Pd exhibited an irreversible anodic peak at  $0.46 \text{ V}$  assigned to the metal-centered oxidation of  $\text{Pd}^{\text{II/III}}$  (Figures S10 and S11). Ru/Pd showed two irreversible anodic peaks at  $0.44$  and  $0.69 \text{ V}$ , as scanned in the  $0.0\text{--}0.9 \text{ V}$  potential range (Figure 3). Scanning the potential to very positive and negative potentials (from  $-2.0$  to  $+2.0 \text{ V}$ ) did not show any addition processes. The oxidation peak at  $0.44 \text{ V}$  is attributed to the metal-centered oxidation of  $\text{Pd}^{\text{II/III}}$ . This redox pair is slightly affected by heteronuclear compound formation. The oxidation peak at  $0.69 \text{ V}$  attributed to the metal-centered  $\text{Ru}^{\text{II/III}}$  couple was cathodically shifted by  $50 \text{ mV}$ , compared with that observed in the mononuclear Ru center. The presence of the two oxidation peaks associated with the Pd and Ru centers confirms that the heterobimetallic complex was obtained.

## 2.2. Polymerization Reactions

Norbornene (NBE) can be polymerized in different ways. Each route leads to its own polymer type, which is different in structure and properties. In this study, the main interest in heterobimetallic complexes lies in their possible application as bifunctional catalysts for the vinyl polymerization and ROMP of NBE. In this sense, mono-Ru, mono-Pd, and Ru/Pd were evaluated as catalytic precursors to produce different poly(NBE)s (Scheme 3). The catalytic behaviors of Ru/Pd and its Pd monometallic fragment (mono-Pd) were investigated in vinyl polymerization under different  $[\text{MAO}]/[\text{Pd}]$  and  $[\text{NBE}]/[\text{Pd}]$  ratios and temperatures ( $30$ ,  $60$ , or  $90^\circ\text{C}$ ). Ru/Pd and its Ru monometallic fragment mono-Ru were evaluated in ROMP reactions under different  $[\text{EDA}]/[\text{Ru}]$  and  $[\text{NBE}]/[\text{Ru}]$  ratios and temperatures ( $25$  or  $50^\circ\text{C}$ ).

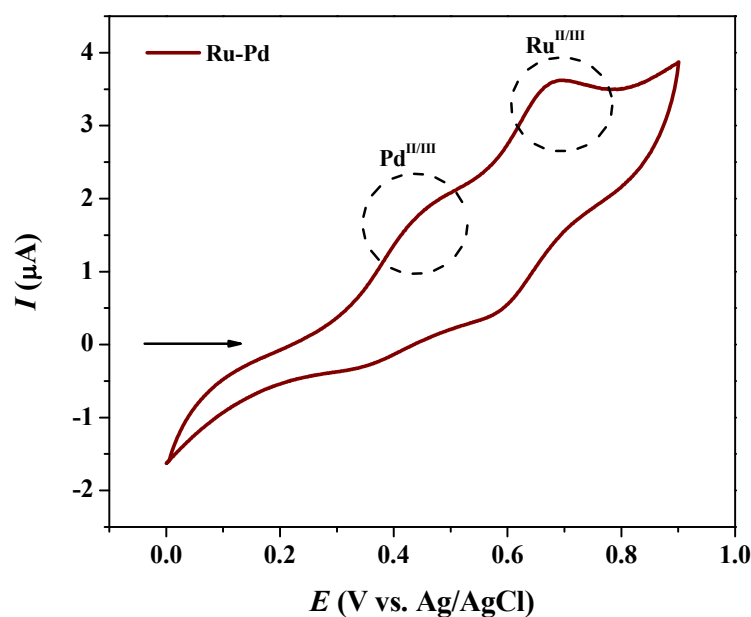
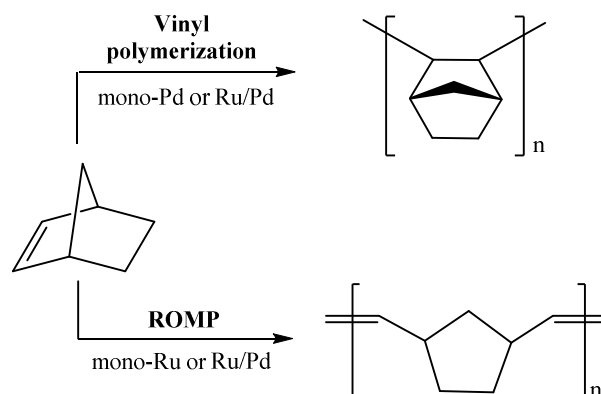


**Figure 3.** Cyclic voltammogram of Ru-Pd obtained in  $n\text{-Bu}_4\text{NPF}_6/\text{CH}_2\text{Cl}_2$  0.1 mol L<sup>-1</sup> vs. Ag/AgCl at a scan rate of 100 mV s<sup>-1</sup>; [Ru/Pd] =  $1.0 \times 10^{-3}$  mol L<sup>-1</sup>.



**Scheme 3.** Schematic representation of different types of polymerizations of NBE.

### 2.2.1. Vinyl Polymerization Reactions

Catalyst activities and polymer yields significantly depended on the applied reaction conditions for the polymerization of NBE, using mono-Pd and Ru/Pd, as shown in Figure 4 and Table 2. Initially, experiments on NBE polymerization were carried out in the absence of MAO (Al), and no catalytic activity for mono-Pd and Ru/Pd was observed (Table 2, Entries 1 and 11). Variation of the Al/mono-Pd and Al/Ru/Pd molar ratio showed considerable effect on the polymerization reaction. The yields of poly(NBE) increased with the increasing the Al/catalyst ratio for both complexes (Figure 4). However, the catalytic activity slightly decreased when the Al/Pd ratio was increased to 3000, since higher amounts of MAO deactivate the catalytic species. The concentration of NBE should meet some conditions to achieve satisfactory polymerization. Greater yields of poly(NBE) were obtained when the NBE/Pd molar ratio was increased from 10,000 to 20,000. Catalytic activity significantly decreased for molar ratios >20,000. Performance of the catalysts was also influenced by reaction temperature, and the highest activity was achieved at 60 °C for Ru/Pd (Table 2, Entry 9). For mono-Pd, quantitative yields were achieved at 30 and 60 °C (Table 2, Entries 9 and 5). A decrease in catalytic activity was observed at higher temperatures (90 °C), probably due to the decomposition of the active species (Table 2, Entry 10 and 20). Under all investigated conditions, mono-Pd showed higher catalytic activity than Ru/Pd. Vinyl polymerization was also performed using mono-

Ru as pre-catalyst to evaluate the contribution of the Ru center to this heterobimetallic complex. The reaction was carried out using  $[Al]/[mono-Ru] = 2500$  and  $[NBE]/[mono-Ru] = 20,000$  molar ratio at  $60\text{ }^{\circ}\text{C}$  for 15 min. The experiment evidenced that the Ru fragment is not able to catalyze NBE vinyl polymerization, since no polymer yield was observed. FTIR analyses of the poly(NBE)s were performed. The characteristic bands of these polymers were similar, at  $\sim 942\text{ cm}^{-1}$ . These absorptions were identified to the ring system of bicyclic heptane [33]. No absorption was observed in the  $735\text{--}960\text{ cm}^{-1}$  range, which is characteristic of the ROMP structure of polyNBEs [34–36]. Therefore, the catalytic polymerization of NBE occurs via vinyl addition.

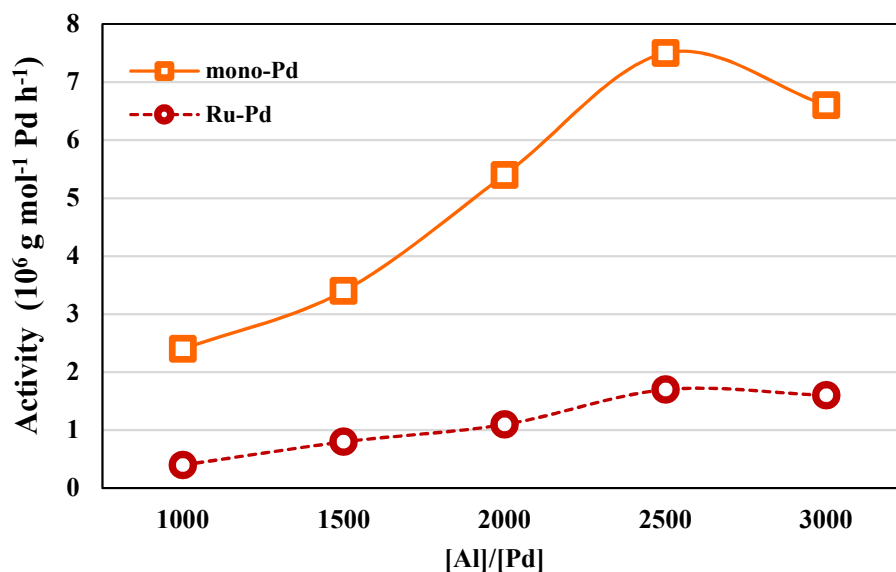


**Figure 4.** Catalytic activity as function of Al/Pd molar ratio.  $V_{\text{total}} = 10\text{ mL}$ ,  $[NBE]/[Pd] = 20,000$ , mono-Pd and Ru/Pd =  $2.5\text{ }\mu\text{mol}$ , and polymerization reaction at  $30\text{ }^{\circ}\text{C}$  for 15 min.

**Table 2.** Polymerization of NBE with mono-Pd and Ru/Pd activated by MAO<sup>a</sup>.

Complex	Entry	Al/Pd	[NBE]/[Pd]	T ( $^{\circ}\text{C}$ )	Activity <sup>b</sup>	Yield (%)
mono-Pd	1	0	20,000	30	-	-
	2	1000	20,000	30	2.4	31.9
	3	1500	20,000	30	3.4	44.7
	4	2000	20,000	30	5.4	72.34
	5	2500	20,000	30	7.5	100
	6	3000	20,000	30	6.6	87.2
	7	2500	10,000	30	3.1	83.0
	8	2500	30,000	30	6.7	59.7
	9	2500	20,000	60	7.5	100
	10	2500	20,000	90	4.0	52.8
Ru/Pd	11	0	20,000	30	-	-
	12	1000	20,000	30	0.4	5.1
	13	1500	20,000	30	0.8	10.4
	14	2000	20,000	30	1.1	14.2
	15	2500	20,000	30	1.7	23.2
	16	3000	20,000	30	1.6	21.7
	17	2500	10,000	30	0.9	23.0
	18	2500	30,000	30	1.0	8.7
	19	2500	20,000	60	3.5	47.0
	20	2500	20,000	90	0.3	3.6

<sup>a</sup> Polymerization conditions:  $V_{\text{total}} = 10\text{ mL}$ ; reaction time: 15 min; complexes:  $2.5\text{ }\mu\text{mol}$ . <sup>b</sup> ( $10^6\text{ g mol}^{-1}\text{ Pd h}^{-1}$ ).

### 2.2.2. ROMP Reactions

Initially, the influence of the Pd-metal center on ROMP reactions was evaluated using mono-Pd as a pre-catalyst, and no polymer yield was observed when  $[NBE]/[mono-Pd] = 3000$  molar ratio and  $V_{EDA} = 10 \mu L$  were employed at  $50^\circ C$  for 30 min. The absence of activity indicates that the Pd fragment has no effect on the ROMP reaction. The use of EDA was indispensable to obtain any ROMP activity. Mono-Ru and Ru/Pd were inactive in the absence of a carbene source. When EDA was added to generate the active species ( $Ru=C$ ), polymer formation was observed. The catalytic activity of mono-Ru and Ru/Pd improved with increasing  $V_{EDA}$  (up to  $V_{EDA} = 5 \mu L$ ) and declined  $V_{EDA} > 5 \mu L$  (Figure 5). An excessive amount of EDA ( $V_{EDA} > 5 \mu L$ ) causes an uncontrolled coordination of EDA to the Ru center, as verified by the decrease in the yields and  $M_n$  values, followed by the increase in the  $D$  values [29,37]. The  $[NBE]/[Ru]$  molar ratio was investigated to achieve the most efficient experimental condition for narrower poly(NBE)s. The yields increase when increasing the  $[NBE]/[Ru]$  molar ratio, starting from 1000, with yields  $< 20\%$ , reaching yields of 59 and 24% at 3000 for mono-Ru and Ru/Pd, respectively (Table 3). A decrease in the yields was observed for  $[NBE]/[Ru] = 5000$ . This behavior has been described in ROMP reactions conducted with similar complexes [18,37–39]. Aiming to reach a more efficient induction period, catalytic tests were also performed at  $50^\circ C$  using the  $[NBE]/[Ru] = 3000$  molar ratio and  $V_{EDA} = 5 \mu L$  for 30 min. The increase in temperature generated higher catalytic activity for mono-Ru and Ru/Pd, which indicates that the induction period depends on the temperature to initiate polymerization (Table 3). For a better understanding of the differences in catalysis using mono-Ru and Ru/Pd, the kinetics of the induction period was investigated by UV-vis from the monitoring of  $\{mono-Ru + EDA \rightarrow mono-Ru=C\}$  and  $\{Ru/Pd + EDA \rightarrow C=Ru/Pd\}$  reactions (Figures S12 and S13). The spectra were recorded every 30 s and  $k_{obs}$  values were determined for mono-Ru and Ru/Pd,  $9.24 \times 10^{-4}$ , and  $7.60 \times 10^{-3} s^{-1}$ , respectively. The similarity in  $k_{obs}$  values indicate that differences in catalytic activity should not be related to the rate of formation of the active species.

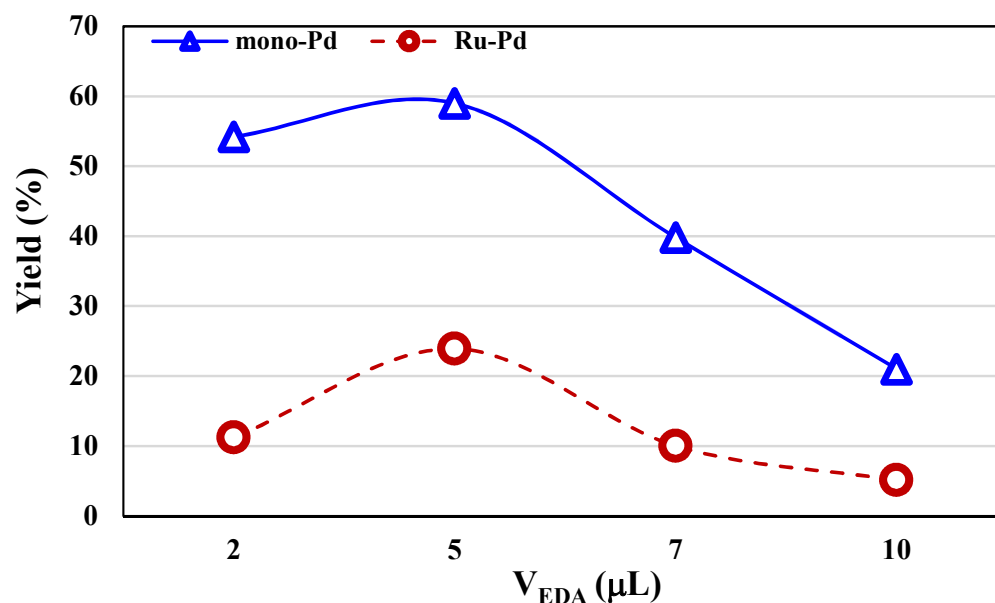


**Figure 5.** Yield dependence as a function  $V_{EDA}$ , at  $25^\circ C$ , for ROMP of NBE with and Ru/Pd in  $CHCl_3$  for 30 min;  $[NBE]/[Ru] = 3000$ .

**Table 3.** ROMP of NBE with mono-Ru and Ru/Pd <sup>a</sup>.

Complex	Entry	V <sub>EDA</sub> (μL)	[NBE]/[Ru]	T (°C)	Yield (%)	M <sub>n</sub> <sup>b</sup> (10 <sup>4</sup> g mol <sup>-1</sup> )	Đ <sup>b</sup>
mono-Ru	1	0	3000	25	-	-	-
	2	2	3000	25	54.2	2.1	1.65
	3	5	3000	25	59.0	5.9	1.53
	4	7	3000	25	39.8	6.8	1.62
	5	10	3000	25	21.6	3.5	1.76
	6	5	1000	25	19.5	2.1	1.48
	7	5	5000	25	28.7	2.7	1.54
	8	5	7000	50	22.6	3.1	1.48
	9	5	3000	50	68.0	5.9	1.61
Ru/Pd	10	0	3000	25	-	-	-
	11	2	3000	25	11.2	2.1	1.63
	12	5	3000	25	23.9	2.9	1.58
	13	7	3000	25	10.4	2.2	1.71
	14	10	3000	25	5.1	1.9	1.79
	15	5	1000	25	8.6	1.8	1.48
	16	5	5000	25	9.9	2.1	1.54
	17	5	7000	50	22.6	3.0	1.48
	18	5	3000	50	31.2	4.5	1.61

<sup>a</sup> Reactions performed in CHCl<sub>3</sub> and 30 min. <sup>b</sup> Determinate by GPC.

Results for the ROMP and vinyl polymerization of NBE showed higher activity using monometallic species as pre-catalysts, compared with that using the heterobimetallic complex. Aiming to find correlations between the structural features and catalytic behaviors of the monometallic and heterobimetallic species, the steric properties of the active species were assessed using computational studies. Steric contour maps illustrate the steric bulk distribution for active species around the Pd- and Ru-metal centers (Figure 6).

As described earlier, the vinyl polymerization is not related to the Ru fragment. In this sense, the Pd center accessibility in the olefin coordination step was investigated, considering the active species for mono-Pd and Ru/Pd. Thus, the chloride and phosphine ligands were removed, and the methyl group was inserted in the Pd center (Figure 5). The difference in the monometallic and heterobimetallic systems is quantified by the percentage of buried volume, % V<sub>Bur</sub>, which is 62.6 for mono-Pd and 63.0 for Ru/Pd. Steric influence on ROMP reactions was evaluated considering the Ru center with the loss of two PPh<sub>3</sub> and addition of EDA to mono-Ru and Ru/Pd (Figure 6). In contrast to the behavior of heterobimetallic complex in vinyl polymerization, a more pronounced difference was found. The % V<sub>Bur</sub> is only 81.4 for mono-Ru and 84.5 for Ru/Pd. As expected, the steric contour maps revealed that the heterobimetallic system is less accessible to the olefin coordination than the corresponding monometallic system.

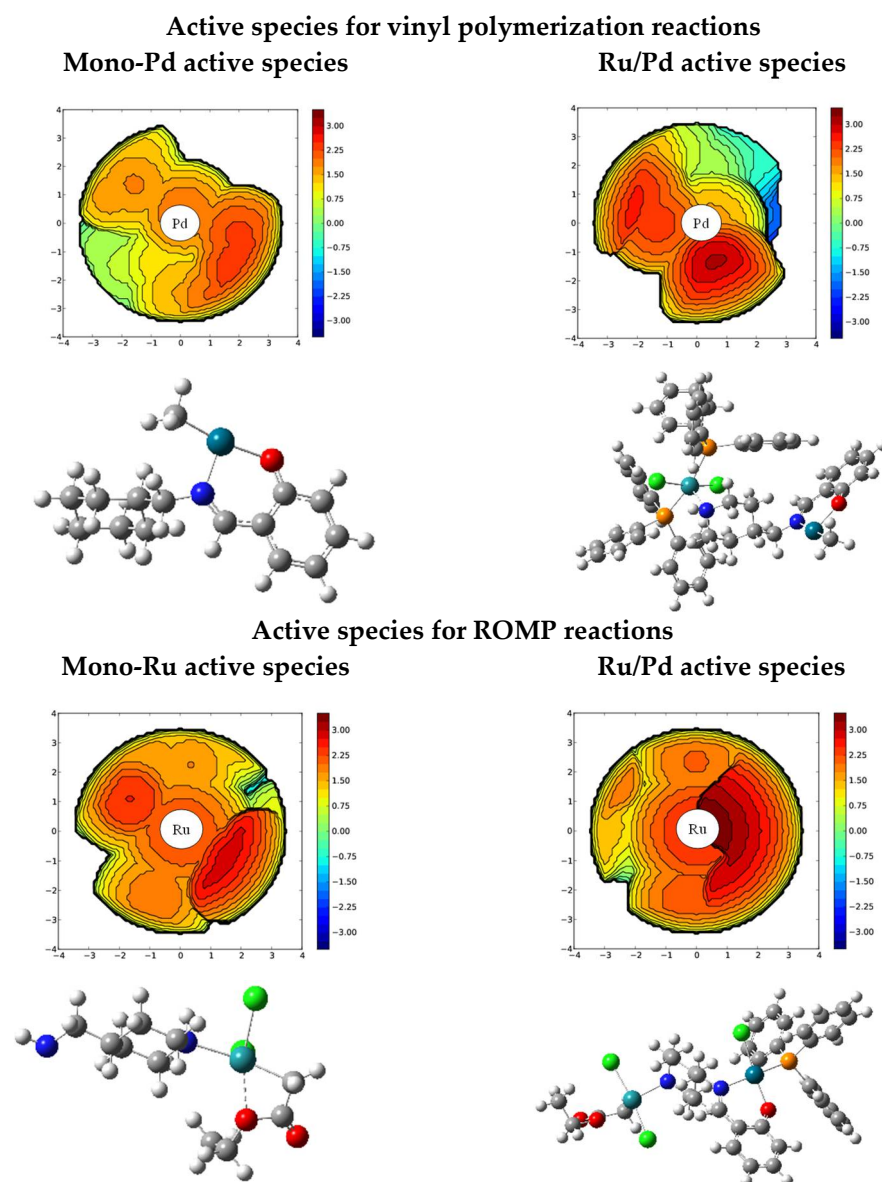


**Figure 6.** Topographic steric maps of active species in vinyl polymerization and ROMP reactions and their respective optimized structures. Active species of mono-Pd and mono-Ru (left) and active species of Ru/Pd (right). The iso-contour curves are in Å.

### 3. Experimental Section

#### 3.1. General Remarks

Unless otherwise stated, all syntheses and manipulations were performed under nitrogen (5.0-nitrogen, Air Liquide) atmosphere, following standard Schlenk techniques. Toluene and dichloromethane ( $\text{CH}_2\text{Cl}_2$ ) were distilled in a calcium hydride system and stored under nitrogen. Norbornene (NBE), ethyldiazoacetate (EDA), 4-(aminomethyl)piperidine (pipNH<sub>2</sub>), salicylaldehyde, methylaluminoxane (MAO), and triphenylphosphine were obtained from Aldrich and used as acquired. The  $[\text{RuCl}_2(\text{PPh}_3)_3]$  and  $[\text{PdCl}_2(\text{PPh}_3)_2]$  complexes were prepared following the literature, and their purity was verified by satisfactory elemental analysis and spectroscopic examination [40,41].

#### 3.2. Analyses

Elemental analyses were performed on a Perkin-Elmer CHN 2400 instrument. Infrared spectra were obtained on a Perkin Elmer Frontier instrument equipped with a diamond

ATR module. The absorption spectra were recorded on a Shimadzu (model UV-1800) spectrophotometer using 1 cm-path length quartz cells. The  $^1\text{H}$  and  $^{31}\text{P}\{^1\text{H}\}$  NMR spectra were obtained on a 500 MHz Bruker Avance III instrument (Bruker BioSpin, Bremen, Germany). Resonance frequency was 500.16 MHz for  $^1\text{H}$  NMR and 202.46 MHz for  $^{31}\text{P}\{^1\text{H}\}$ . Chemical shifts were referenced using TMS and reported in ppm ( $\delta$ ). The analyses were performed in  $\text{CDCl}_3$ . The chemical shifts are listed in ppm downfield of TMS and referenced from the solvent peaks or TMS. The signals were labeled as *s* = singlet, *d* = doublet, *t* = triplet, *q* = quartet, *sept* = septet, and *m* = multiplet. MALDI-TOF analyses were carried out on a Bruker Daltonics Autoflex III Smartbeam. The molecular weights and molecular weight distribution of the polymers were determined by gel permeation chromatography using a Shimadzu Prominence LC system equipped with a LC-20AD pump, DGU-20A5 degasser, CBM-20A communication module, CTO-20A oven at 40 °C, and RID-10A detector equipped with two Shimadzu columns (GPC-805: 30 cm,  $\varnothing$  = 8.0 mm). The retention time was calibrated according to poly(methyl methacrylate) standards using HPLC-grade THF as eluent at 40 °C, with a flow rate of 1.0 mL  $\text{min}^{-1}$ . Electrochemical measurements were performed using an Autolab PGSTAT204 potentiostat with a stationary platinum disk and wire as working and auxiliary electrodes, respectively. The reference electrode was Ag/AgCl. The measurements were performed in  $\text{CH}_2\text{Cl}_2$  with 0.1 mol  $\text{L}^{-1}$  of *n*- $\text{Bu}_4\text{NPF}_6$  at 25 °C  $\pm$  0.1.

### 3.3. Computation Details

The structures of the compounds under study were optimized and had their vibrational frequencies calculated at the density functional theory (DFT) level using the hybrid functional M06 implemented in the Gaussian 09 software and DGDZVP basis set [42–44]. The influence of the solvent on the optimizations was evaluated using the IEFPCM model [45]. The electronic spectra were calculated for the first 30 singlet electronic states, also considering the molecules solvated in dichloromethane (IEFPCM), using the CAM-B3LYP density functional combined with valence triple-zeta quality with double polarized def2-TZVPP basis set [46]. The topographic steric maps of active species in vinyl polymerization and ROMP reactions were obtained using the SambVca 2.1 software [47] from the optimized structures of mono-Pd, mono-Ru and Ru/Pd.

### 3.4. ROMP Procedure

In a typical ROMP experiment, 2.4 or 1.1  $\mu\text{mol}$  of mono-Ru and Ru/Pd, respectively, were dissolved in  $\text{CHCl}_3$  (2 mL) with an appropriate amount of NBE (1.12 g for mono-Ru and 0.53 g for Ru/Pd), followed by addition of a carbene source (EDA). The polymerization was performed for different times (5–60 min). The reaction mixture was stirred at 25 or 50 °C in a silicon oil bath. At room temperature, 10 mL methanol were added, and the precipitated polymer was filtered, washed with methanol, and dried in a vacuum oven at 40 °C, until constant weight was reached. The reported yields are average values from catalytic runs were performed at least three times, and the listed values are the arithmetic averages. The isolated polyNBEs were dissolved in THF for GPC data interpretation.

### 3.5. Vinyl Polymerization Procedure

In a typical procedure, 2.5  $\mu\text{mol}$  of mono-Pd or Ru/Pd in 1.0 mL toluene, 1.80 g of NBE in 3 mL toluene, and an appropriated amount of toluene were added to a Schlenk flask (50 mL) under nitrogen atmosphere. After stirring at 30, 60, or 90 °C for 10 min, a certain amount of MAO was loaded into the polymerization system using a syringe, and the reaction was started. After 15 min, acidic ethanol ( $V_{\text{ethanol}}:V_{\text{conc.HCl}} = 20:1$ ) was added to terminate the reaction. The PNB was isolated by filtration, washed with ethanol, and dried at 100 °C for 24 h under vacuum. For all polymerization procedures, the total reaction volume was 10.0 mL.

### 3.6. Synthesis of $[RuCl_2(PPh_3)_2(piperidine-4(aminomethyl))]$ (mono-Ru)

A 100 mL Schlenk flask equipped with a stirring bar and  $[RuCl_2(PPh_3)_3]$  (0.41 mmol) was purged three times with vacuum/argon cycles. Then, 20 mL acetone, previously purged with Ar(g), was added to the system. The solution was stirred before addition of 4-(aminomethyl)piperidine (0.41 mmol). The mixture was kept at RT for 12 h. Then, the solvent was removed by filtration and the green powder was washed with ethyl ether ( $3 \times 5$  mL) and dried under vacuum for 2 h to give mono-Ru. Elemental analysis for  $C_{42}H_{44}Cl_2N_2Ru$ : calculated C 62.22; H 5.47; N 3.46; found: C 62.48; H 5.83; N 3.21. UV-Vis  $\lambda_{max}$  nm ( $\epsilon_{max}$  [ $10^2$  L mol $^{-1}$  cm $^{-1}$ ]): 230 (1.26), 260 (0.97), 346 (0.15), 640 (0.09). FTIR (cm $^{-1}$ ): 3255  $\nu$ (N-H), 3058  $\nu$ (C-H), 1585–1433  $\nu$ (C=C), 1089  $\nu$ (P-C), 287  $\nu$ (Ru-Cl).  $^1H$  NMR (CDCl $_3$ , 500.16 MHz,  $\delta$ /ppm):  $^1H$  NMR (500.16 MHz, CDCl $_3$ ):  $\delta$  = 7.12–6.70 (m, 30H, CH Ar), 3.75 (t, 2H NH $_2$ ), 3.48 (s, 1H, NH), 3.14–0.48 (m, 11H, CH $_2$  amine) ppm;  $^{31}P\{^1H\}$  NMR (CDCl $_3$ , 202.46 MHz,  $\delta$ ): 62.19, 44.38. MALDI-TOF (CHCl $_3$ ) calcul./found ( $m/z$ ): [mono-Ru]+H $^+$  811,1479/811,1387. EPR: No signal was observed. Yield: 63%.

### 3.7. Synthesis of $[PdCl(PPh_3)(N,O-Schiff)]$ (mono-Pd)

A solution of NaOH (0.05 mmol) in methanol was added to a solution of Schiff base in methanol, and the reaction mixture was stirred at RT for 2 h. The deprotonated ligand mixture was transferred using a cannula to a 50-mL two-necked flask fitted with a reflux condenser containing the  $[PdCl_2(PPh_3)_2]$  (0.05 mmol) precursor. The mixture was stirred and refluxed for 4 h. A dark yellow precipitate was then filtered and washed with methanol and ethyl ether and dried under vacuum. Elemental analysis for  $C_{31}H_{31}ClN_2OPd$ : calculated C 61.40; H 5.15; N 2.31; found: C 61.39; H 5.18; N 2.31. UV-Vis  $\lambda_{max}$  nm ( $\epsilon_{max}$  [ $10^2$  L mol $^{-1}$  cm $^{-1}$ ]): 235 (3.16), 277 (1.29), 343 (0.30), 394 (0.25). FTIR (cm $^{-1}$ ): 3052  $\nu$ (C-H) $_{ar}$ , 2919–2844  $\nu$ (C-H), 1620  $\nu$ (C=N), 1488–1437  $\nu$ (C=C), 1084  $\nu$ (P-C), 352  $\nu$ (Pd-Cl).  $^1H$  NMR (CDCl $_3$ , 500.16 MHz,  $\delta$ /ppm):  $\delta$  = 7.75–7.45 (m, 16H, PPh $_3$ , and H-C=N), 7.27–7.26 (t, 1H, Ph $_{salyc}$ ), 7.24–7.18 (dd, 1H Ph $_{salyc}$ ), 6.90–6.85 (d, 1H Ph $_{salyc}$ ), 6.62–6.56 (t, 1H Ph $_{salyc}$ ), 3.60–3.54 (d, 2H CH $_2$  amine), 2.00–1.90 (m, 1H, C-H amine), 1.90–0.89 (m, 10 H, CH $_2$  amine ring) ppm;  $^{31}P\{^1H\}$  NMR (CDCl $_3$ , 202.46 MHz,  $\delta$ ): 23.22. EPR: No signal was observed. Yield: 86%.

### 3.8. Synthesis of $[RuCl_2(PPh_3)_2](\mu-Schiff)Pd(PPh_3)Cl]$ (Ru/Pd)

Mono-Ru (0.57 mmol) and  $[Pd(PPh_3)_2Cl_2]$  (0.57 mmol) were added to a previously oven-dried 100 mL Schlenk flask equipped with a stirrer, and three vacuum/argon cycles were applied to this system. Then, a previously de-aired solution of salicylaldehyde (0.57 mmol) and dichloromethane was added. The mixture was stirred at RT for 12 h and filtered. The dark red powder was washed with diethyl ether and dried under vacuum for 2 h. Elemental analysis for  $C_{67}H_{62}Cl_3N_2P_3PdOPRu$ : calculated C 61.06; H 4.74; N 2.13; found: C 61.05; H 4.73; N 2.41. UV-Vis  $\lambda_{max}$  nm ( $\epsilon_{max}$  [ $10^2$  L mol $^{-1}$  cm $^{-1}$ ]): 233 (3.80), 355 (0.37), 395 (0.29), 636 (0.07). FTIR (cm $^{-1}$ ): 3264  $\nu$ (N-H); 3052  $\nu$ (C-H) $_{ar}$ , 2964–2869  $\nu$ (C-H), 1622  $\nu$ (C=N), 1481–1437  $\nu$ (C=C), 1083  $\nu$ (P-C), 340  $\nu$ (Pd-Cl), 298  $\nu$ (Ru-Cl).  $^1H$  NMR (CDCl $_3$ , 500.16 MHz,  $\delta$ /ppm): 7.80–6.75 (m, 46 H, PPh $_3$  and H-C=N), 6.78–6.27 (dd, 2H, Ph $_{salyc}$ ), 6.30–6.10 (2t, 2H, Ph $_{salyc}$ ), 3.53–3.45 (m, 1H, secondary amine), 2.00–0.80 (m, 11 H, 5CH $_2$ , 1CH amine).  $^{31}P\{^1H\}$  NMR (CDCl $_3$ , 202.46 MHz,  $\delta$ ): 66.23, 44.18, 38.96, 32.59. MALDI-TOF (CHCl $_3$ ) cal./found ( $m/z$ ):  $-[Ru/Pd+H^+]^+$ : 1317,1292/1317,0373. EPR: No signal was observed. Yield: 64%.

## 4. Conclusions

The new heterobimetallic complex (Ru/Pd) and its monometallic fragments (mono-Ru and mono-Pd) were successfully synthesized and characterized by elemental analysis, spectroscopic techniques, cyclic voltammetry, DFT calculations, and MALDI-TOF. An excellent agreement between theoretically and experimentally calculated UV-*vis* spectra was obtained, which suggests that the Ru moiety presents a square-based pyramidal structure, while the Pd moiety presents a distorted planar square structure. Both fragment structures

were preserved in the bimetallic species. The cyclic voltammetry of Ru/Pd exhibits two irreversible processes at 0.44 and 0.69 V assigned to the Ru<sup>II/III</sup> and Pd<sup>II/III</sup> redox pair, with a slight shift, compared with those from the monometallic species. The Ru/Pd system displays catalytic activity for NBE polymerization via ROMP and addition, reaching yields of 31 and 47%, respectively, in the best observed conditions. The monometallic Ru and Pd fragments proved to be active for NBE polymerization via ROMP (yield of 68%) and addition (quantitative yield). Monometallic systems were more active for both polymerizations, due to their lower hindrance effect, which facilitates olefin coordination.

**Supplementary Materials:** The following supporting information can be downloaded at: <https://www.mdpi.com/article/10.3390/catal12101111/s1>, Figure S1. FTIR spectra of complexes mono-Pd, mono-Ru and Ru/Pd; Figure S2. <sup>1</sup>H NMR spectrum of mono-Ru in CDCl<sub>3</sub>; Figure S3. <sup>1</sup>H NMR spectrum of mono-Pd in CDCl<sub>3</sub>; Figure S4. <sup>1</sup>H NMR spectrum of Ru/Pd in CDCl<sub>3</sub>; Figure S5. <sup>31</sup>P{<sup>1</sup>H} NMR spectrum of mono-Ru in CDCl<sub>3</sub>; Figure S6. <sup>31</sup>P{<sup>1</sup>H} NMR spectrum of mono-Pd in CDCl<sub>3</sub>; Figure S7. <sup>31</sup>P{<sup>1</sup>H} NMR spectrum of mono-Ru in CDCl<sub>3</sub>; Figure S8. MALDI-TOF spectroscopy of mono-Ru from CH<sub>2</sub>Cl<sub>2</sub> solution. Matrix: α-cyano-4-hydroxycinnamic acid; Figure S9. MALDI-TOF spectroscopy of Ru/Pd from CH<sub>2</sub>Cl<sub>2</sub> solution. Matrix: α-cyano-4-hydroxycinnamic acid; Figure S10. Cyclic voltammograms of mono-Ru from CH<sub>2</sub>Cl<sub>2</sub> solutions at 25 °C; Figure S11. Cyclic voltammograms of mono-Pd from CH<sub>2</sub>Cl<sub>2</sub> solutions at 25 °C; Figure S12. Kinetic study of mono-Ru in presence of EDA monitored by electronic spectroscopy every 30 seconds and (insert) dependence of ln(Abs<sub>t</sub> - Abs<sub>inf</sub>) as a function of time at 316 nm; Figure S13. Kinetic study of Ru/Pd in presence of EDA monitored by electronic spectroscopy every 30 seconds and (insert) dependence of ln(Abs<sub>t</sub> - Abs<sub>inf</sub>) as a function of time at 297 nm.

**Author Contributions:** T.R.C. worked on the synthesis and characterization of the complexes, carried out the polymerizations and kinetic experiments, interpreted the results and took the lead in writing the manuscript; G.H.C.M. worked on the synthesis and characterization of the complexes, interpreted the results and took the lead in writing the manuscript; K.A.E.A. performed the <sup>1</sup>H and <sup>31</sup>P{<sup>1</sup>H} NMR experiments and contributed to the final version of the manuscript; A.E.H.M. performed the theoretical studies and contributed to the final version of the manuscript; B.E.G. provided critical feedback and helped shape the research, analysis and manuscript; V.P.C.-J. supervised the project, conceived the study and were in charge of overall direction and planning. All authors have read and agreed to the published version of the manuscript.

**Funding:** This research was funded by São Paulo Research Foundation (FAPESP) 2018/06340-1, 2021/13128-1 (V.P.C.-J.) and 2021/11873-1 (B.E.G.). This work was supported by the Coordenação de Aperfeiçoamento de Pessoal de Nível Superior–Brasil (CAPES)–Finance Code 001.

**Acknowledgments:** We would like to thank Eduardo René Pérez Gonzales (UNESP) and Luana Ribeiro dos Anjos (UNESP) and also to Benedito dos Santos Lima-Neto for their NMR analysis.

**Conflicts of Interest:** The authors declare no conflict of interest.

## References

1. Bender, M.L. *Mechanism of Homogeneous Catalysis from Proton to Proteins*; Wiley: New York, NY, USA, 1971; pp. 19–320.
2. Collman, J.P. Patterns of organometallic reactions related to homogeneous catalysis. *Acc. Chem. Res.* **1968**, *1*, 136–143. [[CrossRef](#)]
3. Singh, K.S. Recent advances in C–H bond functionalization with ruthenium-based catalysts. *Catalysts* **2019**, *9*, 173. [[CrossRef](#)]
4. Montgomery, T.P.; Johns, A.M.; Grubbs, R.H. Recent advancements in stereoselective olefin metathesis using ruthenium catalysts. *Catalysts* **2017**, *7*, 87. [[CrossRef](#)]
5. Clapham, S.E.; Hadzovic, A.; Morris, R.H. Mechanisms of the H<sub>2</sub>-hydrogenation and transfer hydrogenation of polar bonds catalyzed by ruthenium hydride complexes. *Coord. Chem. Rev.* **2004**, *248*, 2201–2237. [[CrossRef](#)]
6. Bellina, F.; Carpita, A.; Rossi, R. Palladium catalysts for the Suzuki cross-coupling reaction: An overview of recent advances. *Synthesis* **2004**, *2004*, 2419–2440. [[CrossRef](#)]
7. Seki, M. Recent advances in Pd/C-catalyzed coupling reactions. *Synthesis* **2006**, *2006*, 2975–2992. [[CrossRef](#)]
8. Kim, A.N.; Stoltz, B.M. Recent advances in homogeneous catalysts for the asymmetric hydrogenation of heteroarenes. *ACS Catal.* **2020**, *10*, 13834–13851. [[CrossRef](#)] [[PubMed](#)]
9. Walter, M.D.; Moorhouse, R.A.; Urbin, S.A.; White, P.S.; Brookhart, M. γ-agostic species as key intermediates in the vinyl addition polymerization of norbornene with cationic (allyl) Pd catalysts: Synthesis and mechanistic insights. *J. Am. Chem. Soc.* **2009**, *131*, 9055–9069. [[CrossRef](#)] [[PubMed](#)]

10. Zhang, Y.; Wang, J. Recent developments in Pd-catalyzed reactions of diazo compounds. *Eur. J. Organ. Chem.* **2011**, *2011*, 1015–1026. [[CrossRef](#)]
11. Gois, P.D.S.; Maia, J.I.P.; Masson, G.H.C.; Martins, D.M.; Machado, A.E.D.H.; Goi, B.E.; Carvalho, V.P.D., Jr. Monometallic and heterobimetallic ruthenium (II) and palladium (II) complexes based on a pyridine-hydrazone ligand as bifunctional catalysts for ROMP of norbornene and ethylene polymerization. *Appl. Organomet. Chem.* **2022**, *36*, 6491. [[CrossRef](#)]
12. Lin, S.-C.A.; Liu, Y.-H.; Peng, S.-M.; Liu, S.-T. Hetero-bimetallic complexes based on an anthridine ligand preparation and catalytic activity. *Organometallics* **2019**, *39*, 123–131. [[CrossRef](#)]
13. Bitzer, M.J.; Kühn, F.E.; Baratta, W. Tandem Suzuki–Miyaura/transfer hydrogenation reaction catalyzed by a Pd–Ru complex bearing an anionic dicarbene. *J. Catal.* **2016**, *338*, 222–226. [[CrossRef](#)]
14. Sabater, S.; Mata, J.A.; Peris, E. Hydrodefluorination of carbon–fluorine bonds by the synergistic action of a ruthenium–palladium catalyst. *Nat. Commun.* **2013**, *4*, 1–7. [[CrossRef](#)]
15. Mata, J.A.; Hahn, F.E.; Peris, E. Heterometallic complexes, tandem catalysis and catalytic cooperativity. *Chem. Sci.* **2014**, *5*, 1723. [[CrossRef](#)]
16. Sun, W.-H.; Yang, H.; Li, Z.; Li, Y. Vinyl polymerization of norbornene with neutral salicylaldiminato nickel (II) complexes. *Organometallics* **2003**, *22*, 3678–3683. [[CrossRef](#)]
17. Calderon, N. Ring-opening polymerization of cycloolefins. *J. Macromol. Sci. Rev. Macromol. Chem.* **1972**, *7*, 105–159. [[CrossRef](#)]
18. Grubbs, R.H. *Handbook of Metathesis*; Wiley-VCH: Weinheim, Germany, 2003; Volume 3.
19. Sutthasupa, S.; Shiotsuki, M.; Sanda, F. Recent advances in ring-opening metathesis polymerization, and application to synthesis of functional materials. *Polym. J.* **2010**, *42*, 905–915. [[CrossRef](#)]
20. Janiak, C.; Paul, G.L. The vinyl homopolymerization of norbornene. *Macromol. Rapid Commun.* **2001**, *22*, 479–493. [[CrossRef](#)]
21. Mathew, J.P.; Reinmuth, A.; Melia, J.; Swords, A.N.; Risse, W. ( $\eta^3$ -allyl) palladium (II) and palladium (II) nitrile catalysts for the addition polymerization of norbornene derivatives with functional groups. *Macromolecules* **1996**, *29*, 2755–2763. [[CrossRef](#)]
22. Liu, H.; Haibin, Y.; Xiaochao, S. Synthesis of nickel and palladium complexes with diarylamido-based unsymmetrical pincer ligands and application for norbornene polymerization. *Dalton Transact.* **2019**, *48*, 609–617. [[CrossRef](#)]
23. Fonseca, L.R.; Sá, J.L.S.; Carvalho, V.P.; Lima-Neto, B.S. Cross-link in norbornadiene-based polymers from ring-opening metathesis polymerization with pyrrolidine-based Ru complex. *Polym. Bull.* **2018**, *75*, 3705–3721. [[CrossRef](#)]
24. Silva, R.A.N.; Borim, P.; Fonseca, L.R.; Lima-Neto, B.S.; Sá, J.L.S.; Carvalho, V., Jr. Non-carbene complex [RuCl<sub>2</sub>(PPh<sub>3</sub>)<sub>2</sub>(azocane)] as active catalyst precursor for ROMP and ATRP. *Catal. Lett.* **2017**, *147*, 1144–1152. [[CrossRef](#)]
25. Afonso, M.B.A.; Cruz, T.R.; Silva, Y.F.; Pereira, J.C.A.; Machado, A.E.; Goi, B.E.; Carvalho, V.P., Jr. Ruthenium (II) complexes of Schiff base derived from cycloalkylamines as pre-catalysts for ROMP of norbornene and ATRP of methyl methacrylate. *J. Organomet. Chem.* **2017**, *851*, 225–234. [[CrossRef](#)]
26. Chaves, H.K.; Ferraz, C.P.; Carvalho, V., Jr.; Lima-Neto, B.S. Tuning the activity of alternative Ru-based initiators for ring-opening metathesis polymerization of norbornene and norbornadiene by the substituent in 4-CH<sub>2</sub>R-piperidine. *J. Mol. Catal. A Chem.* **2014**, *385*, 46–53. [[CrossRef](#)]
27. Cruz, T.R.; Silva, R.A.; Machado, A.E.; Lima-Neto, B.S.; Goi, B.E.; Carvalho, V.P. New dmso–ruthenium catalysts bearing N-heterocyclic carbene ligands for the ring-opening metathesis of norbornene. *New J. Chem.* **2019**, *43*, 6220–6227. [[CrossRef](#)]
28. Masson, G.H.C.; Cruz, T.R.; Gois, P.D.S.; Martins, D.M.; Lima-Neto, B.S.; Oliveira, G.S.; Machado, A.E.H.; Bernardo-Gusmão, K.; Goi, B.E.; Carvalho, V.P., Jr. Ruthenium–nickel heterobimetallic complex as a bifunctional catalyst for ROMP of norbornene and ethylene polymerization. *New J. Chem.* **2021**, *45*, 11466–11473. [[CrossRef](#)]
29. Matos, J.M.E.; Lima-Neto, B.S. Piperidine as an ancillary ligand in the novel [RuCl<sub>2</sub>(PPh<sub>3</sub>)<sub>2</sub>(piperidine)] complex for metathesis polymerization of norbornene and norbornadiene. *J. Mol. Catal. A Chem.* **2004**, *222*, 81–85. [[CrossRef](#)]
30. Fernandes, R.J.; Silva, T.B.; Lima-Neto, B.S.; Haiduke, R.L. Structural and kinetic insights into the mechanism for ring opening metathesis polymerization of norbornene with [RuCl<sub>2</sub>(PPh<sub>3</sub>)<sub>2</sub>(piperidine)] as initiator complex. *J. Mol. Catal. A Chem.* **2015**, *410*, 58–65. [[CrossRef](#)]
31. Cui, J.; Zhang, M.; Zhang, Y. Amino-salicylaldimine–palladium(II) complexes: New and efficient catalysts for Suzuki and Heck reactions. *Inorg. Chem. Commun.* **2010**, *13*, 81–85. [[CrossRef](#)]
32. Agrahari, B.; Layek, S.; Ganguly, R.; Pathak, D.D. Synthesis, crystal structures, and application of two new pincer type palladium (II)-Schiff base complexes in CC cross-coupling reactions. *Inorg. Chim. Acta* **2018**, *471*, 345–354. [[CrossRef](#)]
33. Kennedy, J.P.; Makowski, H.S.J. Carbonium ion polymerization of norbornene and its derivatives. *J. Macromol. Sci. Chem.* **1967**, *1*, 345. [[CrossRef](#)]
34. Barnes, D.A.; Benedikt, G.M.; Goodall, B.L.; Hung, S.S.; Kalamarides, H.A.; Lenhard, S.; McIntosh, L.H.; Selvy, K.T.; Shick, R.A.; Rhodes, L.F. Addition polymerization of norbornene-type monomers using neutral nickel complexes containing fluorinated aryl ligands. *Macromolecules* **2003**, *36*, 2623–2632. [[CrossRef](#)]
35. Patil, A.O.; Zushma, S.; Stibrany, R.T.; Rucker, S.P.; Wheeler, L.M. Vinyl-type polymerization of norbornene by nickel(II) bisbenzimidazole catalysts. *J. Polym. Sci. Part A Polym. Chem.* **2003**, *41*, 2095–2106. [[CrossRef](#)]
36. Zhao, C.; Ribeiro, M.R.; de Pinho, M.N.; Subrahmanyam, V.S.; Gil, C.L.; de Lima, A.P. Structural characteristics and gas permeation properties of polynorbornenes with retained bicyclic structure. *Polymer* **2001**, *42*, 2455–2462. [[CrossRef](#)]
37. Carvalho-Jr, V.; Ferraz, C.P.; Lima-Neto, B.S. Electronic synergism in [RuCl<sub>2</sub>(PPh<sub>3</sub>)<sub>2</sub>(amine)] complexes differing the reactivity for ROMP of norbornene and norbornadiene. *J. Mol. Catal. A Chem.* **2010**, *333*, 46–53. [[CrossRef](#)]

38. Grela, K. (Ed.) *Olefin Metathesis: Theory and Practice*, 1st ed.; Wiley: Hoboken, NJ, USA, 2014.
39. Slugovc, C. The ring opening metathesis polymerisation toolbox. *Macromol. Rapid Commun.* **2004**, *25*, 1283–1297. [[CrossRef](#)]
40. Hallman, P.S.; Stephenson, T.A.; Wilkinson, G. Tetrakis(triphenylphosphine)dichlororuthenium(II) and Tris(triphenylphosphine)dichlororuthenium(II). *Inorg. Synth.* **1970**, *12*, 237.
41. Zahrtmann, N.; Claver, C.; Godard, C.; Riisager, A.; Garcia-Suarez, E.J. Selective oxidative carbonylation of aniline to diphenylurea with ionic liquids. *Chem. Cat. Chem.* **2018**, *10*, 2450–2457. [[CrossRef](#)]
42. Zhao, Y.; Truhlar, D.G. The M06 suite of density functionals for main group thermochemistry, thermochemical kinetics, noncovalent interactions, excited states, and transition elements: Two new functionals and systematic testing of four M06-class functionals and 12 other functionals. *Theor. Chem. Acc.* **2008**, *120*, 215–241.
43. Frisch, M.J.; Trucks, G.W.; Schlegel, H.B.; Scuseria, G.E.; Robb, M.A.; Cheeseman, J.R.; Scalmani, G.; Barone, V.; Mennucci, B.; Petersson, G.A.; et al. *Gaussian 09, Revision E.01*; Gaussian, Inc.: Wallingford, CT, USA, 2013.
44. Godbout, N.; Salahub, D.R.; Andzelm, J.; Wimmer, E. Optimization of Gaussian-type basis sets for local spin density functional calculations. Part I. Boron through neon, optimization technique and validation. *Can. J. Chem.* **1992**, *70*, 560. [[CrossRef](#)]
45. Tomasi, J.; Mennucci, B.; Cancès, E. The IEF version of the PCM solvation method: An overview of a new method addressed to study molecular solutes at the QM ab initio level. *J. Mol. Struct. Theochem.* **1999**, *464*, 211–226. [[CrossRef](#)]
46. O'Boyle, N.M.; Tenderholt, A.L.; Langner, K.M. cclib: A library for package-independent computational chemistry algorithms. *Comp. Chem.* **2007**, *29*, 839–845. [[CrossRef](#)] [[PubMed](#)]
47. Falivene, L.; Cao, Z.; Petta, A.; Serra, L.; Poater, A.; Oliva, R.; Cavallo, L. Towards the online computer-aided design of catalytic pockets. *Nat. Chem.* **2019**, *1*, 872–879. [[CrossRef](#)] [[PubMed](#)]